Thermodynamics and efficiency of sequentially collisional Brownian particles: The role of drivings

Fernando S. Filho,[1] Bruno A. N. Akasaki,[1] Carlos E. F. Noa,[1] Bart Cleuren,[2] and Carlos E. Fiore[1]
[1]*Universidade de São Paulo, Instituto de Física, Rua do Matão, 1371, 05508-090 São Paulo, SP, Brasil*
[2]*UHasselt, Faculty of Sciences, Theory Lab, Agoralaan, 3590 Diepenbeek, Belgium*

(Received 13 June 2022; accepted 30 September 2022; published 24 October 2022)

Brownian particles placed sequentially in contact with distinct thermal reservoirs and subjected to external driving forces are promising candidates for the construction of reliable engine setups. In this contribution, we address the role of driving forces for enhancing the collisional machine performance. Analytical expressions for thermodynamic quantities such as power output and efficiency are obtained for general driving schemes. A proper choice of these driving schemes substantially increases both power output and efficiency and extends the working regime. Maximizations of power and efficiency, whether with respect to the strength of the force, driving scheme, or both have been considered and exemplified for two kind of drivings: generic power-law and harmonic (sinusoidal) drivings.

DOI: 10.1103/PhysRevE.106.044134

I. INTRODUCTION

The construction of nanoscale engines has received a great deal of attention and recent technological breakthroughs have made feasible not only the realization of distinct setups composed of quantum dots [1], colloidal particles [2–5], single and coupled systems [6–8] but also coarse-grained approaches for systems presenting different degrees of freedom [9,10]. In contrast with their macroscopic counterparts, their main features are strongly influenced by fluctuations when operating at the nanoscale, having several features described within the framework of stochastic thermodynamics [11–16].

Recently a novel approach, coined collisional, has been put forward as a candidate for the realization of reliable thermal engines [17,18] and novel engine setups [19–21]. They consist of sequentially placing the system (a Brownian particle) in contact with distinct thermal reservoirs and subjected to external driving forces during each stage (stroke) of the cycle. Each stage is characterized by the temperature of the connected thermal reservoir and the external driving force. The time needed to switch between the thermal baths at the end of each stage is neglected. Despite its reliability in distinct situations, such as systems interacting only with a small fraction of the environment and those presenting distinct drivings over each member of the system [22–25], the engine can operate rather inefficiently depending on the way it is projected (temperatures, kind of driving, and duration of each stroke). Hence the importance for strategies to enhance its performance [20,21]. Among the distinct approaches, we cite those based on the maximization of power [1,6,14,26–33], efficiency [20,34,35], low or finite dissipation [36,37] and even the assumption of maximization via the largest dissipation [38].

This paper deals with the above points but it focuses on a different direction, namely, the optimization of the engine performance by fine-tuning the driving at each stroke. Such an idea is illustrated in a collisional Brownian machine, which has been considered as a working substance in several works, both from the theoretical [7,39–43] and experimental points of view [3,35,44–46]. The collisional description allows us to derive general (and exact) expressions for thermodynamic quantities, such as output power and efficiency, irrespective of the kind of driving [20]. To exploit the consequences of a distinct driving each stroke and possible optimizations, two representative examples will be considered: generic harmonic and power-law drivings. The former consists of a simpler and feasible way to drive Brownian particles out of equilibrium [35,45,47–49] and providing simultaneous maximizations of the engine [7]. Since the engine performance is substantially reduced for linear drivings when compared with constant ones [19,20], generic power-law drivings have been considered not only for generalizing the machine performance beyond constant and linear drivings but also to exploit the possibility of obtaining a gain by changing its form at each stroke.

This paper is organized as follows: Section II presents the model and the main expressions for the thermodynamic quantities. Efficiency and optimization is discussed in detail for both classes of drivings in Sec. III. Conclusions and perspectives are addressed in Sec. IV.

II. THERMODYNAMICS AND MAIN EXPRESSIONS

We focus on the simplest projection of an engine composed of only two strokes and returning to the initial step after one cycle. The time it takes to complete one cycle is set to τ, with each stroke $\in\{1, 2\}$ lasting a time $\tau/2$. During stroke i the Brownian particle of mass m is in contact with a thermal bath at temperature T_i and described by the Langevin equation.[1]

$$\frac{dv_i(t)}{dt} = -\gamma_i v_i(t) + \tilde{f}_i(t) + \zeta_i(t), \tag{1}$$

[1]Eq. (1) is formally identical to description of the overdamped harmonic oscillator subject to the harmonic force $\bar{f}_h = -\bar{k}x$ just by replacing $x \to v$, $\bar{k}/\alpha \to \gamma_i$, $1/\alpha \to \gamma_i/m$.

where γ_i and $\tilde{f}_i(t)$ denote the viscous coefficient and an external force by mass, respectively, where for simplicity the driving is independent on the position and velocity. The interaction between the particle and thermal bath (at temperature T_i) is represented by a stochastic force (per mass) $\zeta_i(t)$ fulfilling the following (white noise) properties: $\langle\zeta_i(t)\rangle = 0$ and $\langle\zeta_i(t')\zeta_j(t)\rangle = 2\gamma_i k_B T_i \delta_{ij}\delta(t'-t)/m$.

To introduce thermodynamic forces and fluxes, we start from the expression for the steady entropy production (averaged over a complete period) given by $\overline{\sigma} = \overline{\dot{Q}}_1/T_1 + \overline{\dot{Q}}_2/T_2$, where $\overline{\dot{Q}}_1$ and $\overline{\dot{Q}}_2$ are the exchanged heat during strokes 1 and 2, respectively. By resorting to the first law of thermodynamics $\overline{\dot{Q}}_1 + \overline{\dot{Q}}_2 = -(\overline{\dot{W}}_1 + \overline{\dot{W}}_2)$ and expressing T_1 and T_2 in terms of the mean $T = (T_1 + T_2)/2$ and the difference $\Delta T = T_2 - T_1$, in such a way that $\overline{\sigma}$ can be rewritten in the following (general) form:

$$\overline{\sigma} = \frac{4T^2}{4T^2 - \Delta T^2}\left[-\frac{1}{T}(\overline{\dot{W}}_1 + \overline{\dot{W}}_2) + (\overline{\dot{Q}}_1 - \overline{\dot{Q}}_2)\frac{\Delta T}{2T^2}\right]. \quad (2)$$

Expressions for work, heat, and entropy production are obtained by taking the associate Fokker-Planck (FP) equation to Eq. (1), in which the time evolution of probability distribution $P_i(v,t)$ is given by [15,50,51]

$$\frac{\partial P_i}{\partial t} = -\frac{\partial J_i}{\partial v} - \tilde{f}_i(t)\frac{\partial P_i}{\partial v}, \quad (3)$$

where J_i denotes the probability current given by

$$J_i = -\gamma_i v P_i - \frac{\gamma_i k_B T_i}{m}\frac{\partial P_i}{\partial v}. \quad (4)$$

Applying the usual boundary conditions in the space of velocities, in which both $P_i(v,t)$ and $J_i(v,t)$ vanish as $|v| \to \infty$, the time evolution of the system energy $U_i(t) = m\langle v_i^2\rangle/2$ during each stroke corresponds to the sum of two terms:

$$\frac{d}{dt}U_i(t) = -[\dot{W}_i(t) + \dot{Q}_i(t)], \quad (5)$$

with the mean power $\dot{W}_i(t)$ and heat $\dot{Q}_i(t)$ given by

$$\dot{W}_i(t) = -m\langle v_i\rangle(t)\tilde{f}_i(t), \quad (6)$$

$$\dot{Q}_i(t) = \gamma_i\left(m\langle v_i^2\rangle(t) - k_B T_i\right). \quad (7)$$

By averaging over a complete period, one recovers the first law of thermodynamics, as stated previously. Similarly, the time evolution of the system entropy $S_i(t) = -k_B\langle \ln P_i\rangle$ during stage i can be expressed as a difference between two terms:

$$\frac{d}{dt}S_i = \sigma_i(t) - \Phi_i(t), \quad (8)$$

where $\sigma_i(t)$ and $\Phi_i(t)$ are the entropy production rate and the entropy flux, respectively, whose expressions are given by

$$\sigma_i(t) = \frac{m}{\gamma_i T_i}\int \frac{J_i^2}{P_i}dv \quad \text{and} \quad \Phi_i(t) = \frac{\dot{Q}_i(t)}{T_i}. \quad (9)$$

Note that the right side of Eq. (9) integrated over a complete period is equivalent with the relation for $\overline{\sigma}$ given by Eq. (2) and it is strictly positive in the time-periodic state [52]. Such class of systems evolve to a nonequilibrium steady state whose probability distribution $P_i(v,t)$ for the ith stage, satisfying Eq. (3), is Gaussian,

$$P_i(v,t) = \exp\{-[v - \langle v_i\rangle(t)]^2/2b_i(t)\}/\sqrt{2\pi b_i(t)}, \quad (10)$$

in which the mean $\langle v_i\rangle(t)$ and variance $b_i(t) = \langle v_i^2\rangle(t) - \langle v_i\rangle^2(t)$ are time dependent and determined by the following equations:

$$\frac{d\langle v_i\rangle(t)}{dt} = -\gamma_i\langle v_i\rangle(t) + \tilde{f}_i(t), \quad (11)$$

and

$$\frac{db_i(t)}{dt} = -2\gamma_i b_i(t) + \frac{2\gamma_i k_B T_i}{m}, \quad (12)$$

respectively. To obtain explicit and general results, the external forces will be expressed in the following form:

$$\tilde{f}_i(t) = \begin{cases} X_1 g_1(t), & t \in [0, \tau/2] \\ X_2 g_2(t), & t \in [\tau/2, \tau], \end{cases} \quad (13)$$

where $g_i(t)$ and X_i account for the kind of driving and its strength at stage i, respectively. It is worth mentioning that Eq. (13) describes generic drivings which do not depend on the velocity or position of the Brownian particle. Continuity of $P_i(v,t)$ at times $t = \tau/2$ and $t = \tau$ implies

$$\langle v_1\rangle(\tau/2) = \langle v_2\rangle(\tau/2), \quad b_1(\tau/2) = b_2(\tau/2), \quad (14)$$

$$\langle v_1\rangle(0) = \langle v_2\rangle(\tau), \quad b_1(0) = b_2(\tau). \quad (15)$$

From the above, we arrive at the following general expressions (evaluated for $k_B = 1$ and $\gamma_1 = \gamma_2 \equiv \gamma$):

$$\langle v_1\rangle(t) = X_1\int_0^t e^{\gamma(t'-t)}g_1(t')dt' + \frac{1}{e^{\gamma\tau}-1}\left\{X_1\int_0^{\tau/2} e^{\gamma(t'-t)}g_1(t')dt' + X_2\int_{\tau/2}^{\tau} e^{\gamma(t'-t)}g_2(t')dt'\right\}, \quad (16)$$

$$\langle v_2\rangle(t) = X_2\int_{\tau/2}^t e^{\gamma(t'-t)}g_2(t')dt' + \frac{1}{e^{\gamma\tau}-1}\left\{e^{\gamma\tau}X_1\int_0^{\tau/2} e^{\gamma(t'-t)}g_1(t')dt' + X_2\int_{\tau/2}^{\tau} e^{\gamma(t'-t)}g_2(t')dt'\right\}, \quad (17)$$

$$b_1(t) = -\frac{1}{m}\frac{(T_1 - T_2)}{(1+e^{-\gamma\tau})}e^{-2\gamma t} + \frac{T_1}{m}, \quad b_2(t) = -\frac{1}{m}\frac{(T_2 - T_1)}{(1+e^{-\gamma\tau})}e^{-2\gamma(t-\tau/2)} + \frac{T_2}{m}. \quad (18)$$

Inserting the above expressions into Eqs. (6) and (7) and averaging over a complete cycle, we finally arrive at

$$\overline{\dot{W}}_1 = -\frac{m}{\tau(e^{\gamma\tau}-1)}\Bigg[X_1^2\Bigg((e^{\gamma\tau}-1)\int_0^{\tau/2} g_1(t)e^{-\gamma t}\int_0^t g_1(t')e^{\gamma t'}\,dt'dt + \int_0^{\tau/2} g_1(t)e^{-\gamma t}\,dt\int_0^{\tau/2} g_1(t')e^{\gamma t'}\,dt'\Bigg) + X_1X_2\int_0^{\tau/2} g_1(t)e^{-\gamma t}\,dt\int_{\tau/2}^{\tau} g_2(t')e^{\gamma t'}\,dt'\Bigg], \tag{19}$$

$$\overline{\dot{Q}}_1 = \frac{\gamma m}{\tau}\Bigg[\int_0^{\tau/2}\langle v_1\rangle^2 dt - \frac{1}{2\gamma m}\tanh(\gamma\tau/2)(T_1-T_2)\Bigg], \tag{20}$$

and

$$\overline{\dot{W}}_2 = -\frac{m}{\tau(e^{\gamma\tau}-1)}\Bigg[X_2^2\Bigg(\int_{\tau/2}^{\tau} g_2(t)e^{-\gamma t}dt\int_{\tau/2}^{\tau} g_2(t')e^{\gamma t'}dt' + (e^{\gamma\tau}-1)\int_{\tau/2}^{\tau} g_2(t)e^{-\gamma t}\int_{\tau/2}^{t} g_2(t')e^{\gamma t'}dt'dt\Bigg) + X_1X_2e^{\gamma\tau}\Bigg(\int_{\tau/2}^{\tau} g_2(t)e^{-\gamma t}\,dt\int_0^{\tau/2} g_1(t')e^{\gamma t'}\,dt'\Bigg)\Bigg], \tag{21}$$

$$\overline{\dot{Q}}_2 = \frac{m\gamma}{\tau}\Bigg[\int_{\tau/2}^{\tau}\langle v_2\rangle^2 dt + \frac{1}{2\gamma m}\tanh(\gamma\tau/2)(T_1-T_2)\Bigg], \tag{22}$$

for first and second stages, respectively, and $\overline{\sigma}$ is promptly obtained by inserting the above expressions into Eq. (2). It is worth emphasizing that Eqs. (19)–(22) are general and valid for any kind of drivings and temperatures. Close to equilibrium the entropy production [Eq. (2)] assumes the familiar *flux times force* form $\overline{\sigma} \approx J_1f_1 + J_2f_2 + J_Tf_T$ where

$$f_1 = X_1/T, \quad f_2 = X_2/T, \quad f_T = \Delta T/T^2 \tag{23}$$

($\Delta T = T_2 - T_1$) and fluxes defined by

$$\overline{\dot{W}}_1 = -TJ_1f_1, \quad \overline{\dot{W}}_2 = -TJ_2f_2, \quad \overline{\dot{Q}}_1 - \overline{\dot{Q}}_2 = 2J_T. \tag{24}$$

Up to first order in the forces these fluxes can be expressed in terms of Onsager coefficients $J_1 = L_{11}f_1 + L_{12}f_2$, $J_2 = L_{21}f_1 + L_{22}f_2$, and $J_T = L_{TT}f_T$ which results in

$$L_{11} = \frac{mT}{\tau(e^{\gamma\tau}-1)}\Bigg[(e^{\gamma\tau}-1)\int_0^{\tau/2} g_1(t)e^{-\gamma t}\int_0^t g_1(t')e^{\gamma t'}dt'dt + \int_0^{\tau/2} g_1(t)e^{-\gamma t}dt\int_0^{\tau/2} g_1(t')e^{\gamma t'}dt'\Bigg], \tag{25}$$

$$L_{22} = \frac{mT}{\tau(e^{\gamma\tau}-1)}\Bigg[\int_{\tau/2}^{\tau} g_2(t)e^{-\gamma t}dt\int_{\tau/2}^{\tau} g_2(t')e^{\gamma t'}dt' + (e^{\gamma\tau}-1)\int_{\tau/2}^{\tau} g_2(t)e^{-\gamma t}\int_{\tau/2}^{t} g_2(t')e^{\gamma t'}dt'dt\Bigg], \tag{26}$$

$$L_{12} = \frac{mT}{\tau(e^{\gamma\tau}-1)}\int_0^{\tau/2} g_1(t)e^{-\gamma t}dt\int_{\tau/2}^{\tau} g_2(t')e^{\gamma t'}dt', \quad L_{21} = \frac{mTe^{\gamma\tau}}{\tau(e^{\gamma\tau}-1)}\int_0^{\tau/2} g_1(t')e^{\gamma t'}dt'\int_{\tau/2}^{\tau} g_2(t)e^{-\gamma t}dt, \tag{27}$$

$$L_{TT} = \frac{T^2}{2\tau}\tanh\left(\frac{\gamma\tau}{2}\right). \tag{28}$$

Four remarks are in order. First, Eqs. (19) and (21) state that average powers are independent of the velocities. Second, Onsager coefficients L_{ij} $(i, j = 1, 2)$ are exact and valid for arbitrary values of f_i. Third, to verify Onsager-Casimir symmetry for the cross coefficients L_{12} and L_{21} it is necessary not only to reverse the drivings but also to exchange the indices $1 \leftrightarrow 2$, as argued in Ref. [18]. Fourth and last, there is no coupling between work fluxes and heat flux. That is, the cross coefficients L_{T1}, L_{1T}, L_{T2}, and L_{2T} are absent. Hence this class of engines does not convert heat into work (nor work is converted into heat) and always loses its efficiency when the difference of temperatures ΔT between thermal baths is large, because heat cannot be converted into output work [7,20]. As we shall see further, for the regime of equal or "low" temperatures, efficiency properties can be solely expressed in terms of Onsager coefficients and their derivatives.

III. EFFICIENCY

As stated before, our aim is to adjust the drivings in order to optimize the system performance. More concretely, given an amount of energy injected to the system, whether in the form of input work $\overline{\dot{W}}_{\rm in} \equiv \overline{\dot{W}}_1 < 0$ and/or heat $\overline{\dot{Q}}_{\rm in} = \overline{\dot{Q}}_1\Theta(-\overline{\dot{Q}}_1) + \overline{\dot{Q}}_2\Theta(-\overline{\dot{Q}}_2) < 0$ [$\Theta(x)$ denoting the Heaviside function], it is partially converted into power output $\mathcal{P} \equiv \overline{\dot{W}}_2 \geqslant 0$. A measure of such conversion is characterized by the efficiency, given as the ratio between the above quantities:

$$\eta = -\frac{\mathcal{P}}{\overline{\dot{W}}_{\rm in} + \overline{\dot{Q}}_{\rm in}}. \tag{29}$$

To gain insight on the role of driving, we shall split the analysis in two parts, focusing first on the isothermal setup.

A. Overview on Brownian work-to-work converters and distinct maximization routes

Work-to-work converters have been studied broadly in the context of biological motors such as kinesin [53–55] and myosin, in which chemical energy is converted into mechanical and vice versa [56]. More recently, distinct work-to-work converters made of Brownian engines have attracted

considerable attention, and in this section we briefly review their main aspects [7,19,20,35,57]. Setting $\Delta T = 0$ ($f_T = 0$) implies that $\overline{\dot{Q}_{\rm i}} \geqslant 0$ and hence Eq. (29) reduces to the standard common definition of efficiency given by the ratio between entropy production components $-J_2 f_2/J_1 f_1$ and expressed in terms of the ratio between Onsager coefficients [7,19,20]:

$$\eta \equiv -\frac{\mathcal{P}}{\overline{\dot{W}}_{\rm in}} = -\frac{J_2 f_2}{J_1 f_1} = -\frac{L_{22} f_2^2 + L_{21} f_1 f_2}{L_{12} f_1 f_2 + L_{11} f_1^2}. \tag{30}$$

For any kind of driving and period, the engine regime $\mathcal{P} > 0$ implies that the absolute value for the output force f_2 must lie in the interval $0 \leqslant |f_2| \leqslant |f_m|$, where $f_m = -L_{21} f_1/L_{22}$. Since power, efficiency, and dissipation are not independent from each other, f_m can be related with f_{2mS} (keeping f_1 and driving parameter constant), for which the average entropy production $\bar{\sigma} = L_{11} f_1^2 + (L_{12} + L_{21}) f_1 f_2 + L_{22} f_2^2$ is minimal. It is straightforward to show that $f_m = f_{2mS} + (L_{12} - L_{21}) f_1/(2L_{22})$. Note that $f_m = f_{2mS}$ only when the Onsager coefficients are symmetric, $L_{12} = L_{21}$.

Optimized quantities, whether power and efficiency, can be obtained under three distinct routes: optimization with respect to (i) the output force f_2 (keeping f_1 and a driving parameter δ fixed), (ii) the driving parameter δ (forces f_1 and f_2 held fixed), and (iii) a simultaneous optimization with respect to both f_2 and δ. As discussed in Refs. [19,20,35], such optimized quantities can be expressed in terms of Onsager coefficients and their derivatives.

The former case (maximization with respect to the output force) is similar to findings from Refs. [19,20,35], in which the maximum power $\mathcal{P}_{MP,f_2}$ (with efficiency η_{MP,f_2}) and maximum efficiency η_{ME,f_2} (with power $\mathcal{P}_{ME,f_2}$) are obtained via optimal adjustments f_{2MP} and f_{2ME}. By taking the derivative of $\mathcal{P}$ and Eq. (30) with respect to f_2 and setting them equal to zero, f_{2ME} and f_{2MP} are given by

$$\frac{f_{2ME}}{f_1} = \frac{L_{11}}{L_{12}}\left(\sqrt{1 - \frac{L_{12}L_{21}}{L_{11}L_{22}}} - 1\right) \quad \text{and} \quad \frac{f_{2MP}}{f_1} = \frac{-L_{21}}{2L_{22}}, \tag{31}$$

and their associate efficiencies read

$$\eta_{ME,f_2} = -\frac{L_{21}}{L_{12}} + \frac{2L_{11}L_{22}}{L_{12}^2}\left(1 - \sqrt{1 - \frac{L_{12}L_{21}}{L_{11}L_{22}}}\right), \tag{32}$$

and

$$\eta_{MP,f_2} = \frac{L_{21}^2}{4L_{11}L_{22} - 2L_{12}L_{21}}, \tag{33}$$

respectively. Analogous expressions for the power at maximum efficiency $\mathcal{P}_{ME,f_2}$ and the maximum power $\mathcal{P}_{MP,f_2}$ can obtained by inserting f_{2ME} or f_{2MP} into the expression for $\mathcal{P}$. As stated before, the second maximization to be considered is carried out for fixed output forces and a given driving parameter δ is adjusted ensuring maximum power δ_{MP} and/or efficiency δ_{ME}, respectively. According to Refs. [7,20], they fulfill the following expressions:

$$\frac{L'_{21}(\delta_{MP})}{L'_{22}(\delta_{MP})} = -\frac{f_2}{f_1}, \tag{34}$$

and

$$\Delta_{2212}(\delta_{ME}) f_2^2 + \Delta_{2111}(\delta_{ME}) f_1^2 + [\Delta_{2211}(\delta_{ME}) + \Delta_{2112}(\delta_{ME})] f_1 f_2 = 0, \tag{35}$$

respectively, where $L'_{ij}(\delta) \equiv \partial L_{ij}(\delta)/\partial\delta$ is the derivative of coefficient L_{ij} with respect to the driving parameter δ and $\Delta_{ijkl}(\delta) = L'_{ij}(\delta) L_{kl}(\delta) - L'_{kl}(\delta) L_{ij}(\delta)$. Associate maximum power and efficiency are given by

$$\mathcal{P}_{MP,\delta} = \frac{L'_{21}(\delta_{MP})}{L'^2_{22}(\delta_{MP})}\Big[L_{21}(\delta_{MP}) L'_{22}(\delta_{MP}) - L_{22}(\delta_{MP}) L'_{21}(\delta_{MP})\Big] f_1^2, \tag{36}$$

and

$$\eta_{ME,\delta} = -\frac{L_{22}(\delta_{ME}) f_2^2 + L_{21}(\delta_{ME}) f_1 f_2}{L_{11}(\delta_{ME}) f_1^2 + L_{12}(\delta_{ME}) f_1 f_2}, \tag{37}$$

respectively, and expressions for $\mathcal{P}_{ME,\delta}$ and $\eta_{MP,\delta}$ are obtained in a similar way. Although exact and valid for any choice of the drivings $g_i(t)$ and forces f_i, Eqs. (34) and (35), in general, have to be solved numerically to obtain δ_{MP} and δ_{ME}.

In certain cases (as shall be explained next), it is possible to maximize the engine with respect to the output force f_2 and a driving parameter δ simultaneously, which corresponds to the crossing point between maximum lines (power or efficiency) with respect to f_2 and δ. More specifically, given the locus of maxima f_{2MP}/f_{2ME} (δ fixed) and δ_{MP}/δ_{ME} (f_2 fixed), the global $\delta^*_{MP}/\delta^*_{ME}$ and f^*_{2MP}/f^*_{2ME} corresponds to their intersection. For instance, the global maximization of power is given

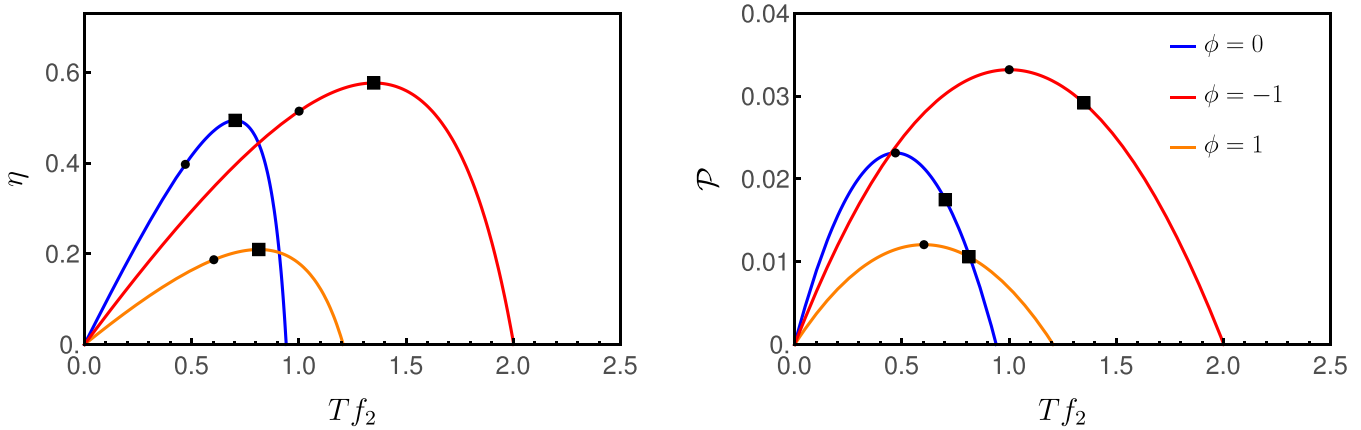

FIG. 1. For harmonic drivings, the depiction of efficiency η and power-output $\mathcal{P}$ versus output force $X_2 = T f_2$ for distinct ϕ. In each panel, from left to right curves, results for $\phi = 0$, -1, and 1, respectively. Squares and circles denote the maximum efficiencies and power outputs, according to Eqs. (32) and (31). In all cases, we set $X_1 = T f_1 = 1$, $\tau = 2$, $\gamma = k_B = m = 1$, and $T = 1/2$.

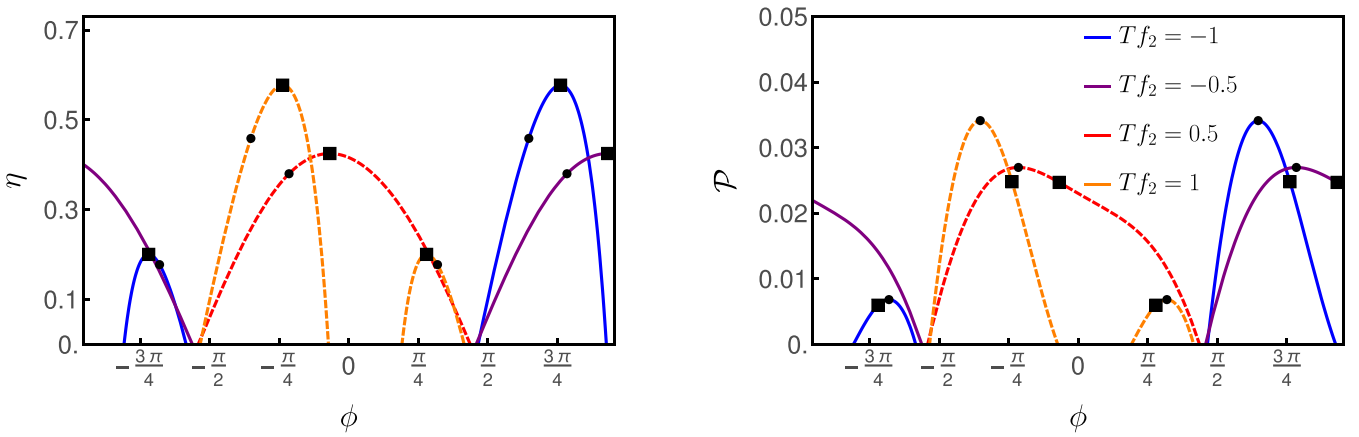

FIG. 2. For $\tau = 2$ and distinct Tf_2, the depiction of efficiency η and power-output $\mathcal{P}$ versus ϕ. In each panel, from left to right curves, results for $Tf_2 = -0.5, -1, 0.5$, and 1, respectively. Squares and circles denote the maximum efficiencies and powers, respectively, according to Eqs. (34) and (35). In all cases, we set $X_1 = Tf_1 = 1$, $\gamma = k_B = m = 1$, and $T = 1/2$.

by Eqs. (31) and (34):

$$\frac{L'_{21}(\delta^*_{MP})}{L'_{22}(\delta^*_{MP})} = \frac{1}{2}\frac{L_{21}(\delta^*_{MP})}{L_{22}(\delta^*_{MP})} \quad \text{and} \quad \frac{f^*_{2MP}}{f_1} = -\frac{1}{2}\frac{L_{21}(\delta^*_{MP})}{L_{22}(\delta^*_{MP})}, \tag{38}$$

whose (associate global) maximum power $\mathcal{P}^*$ and efficiency η^*read

$$\mathcal{P}^* = \frac{1}{4}\frac{L^2_{21}(\delta^*_{MP})}{L_{22}(\delta^*_{MP})} f_1^2, \tag{39}$$

and

$$\eta^* = \frac{L^2_{21}(\delta^*_{MP})}{4L_{11}(\delta^*_{MP})L_{22}(\delta^*_{MP}) - 2L_{21}(\delta^*_{MP})L_{12}(\delta^*_{MP})}, \tag{40}$$

respectively.

B. Applications

With the main expressions introduced, we are now in a position to analyze the role of driving in our two-stage engine. As stated in the Introduction, we shall consider two distinct (but exhibiting complementary features) cases: generic harmonic and power-law drivings. Besides the feasible experimental implementation [35,58,59], harmonic (sinusoidal) drivings can provide simultaneous maximization of an engine composed of two interacting Brownian particles by tuning the phase difference between harmonic drivings and their strengths [7]. In this contribution, we address a simultaneous maximization for our collisional engine. Conversely, power-law drivings has been considered in order to generalize the machine performance beyond constant and linear drivings as well as by exploiting the possibility of improving the engine performance via distinct drivings at each stage [19,20].

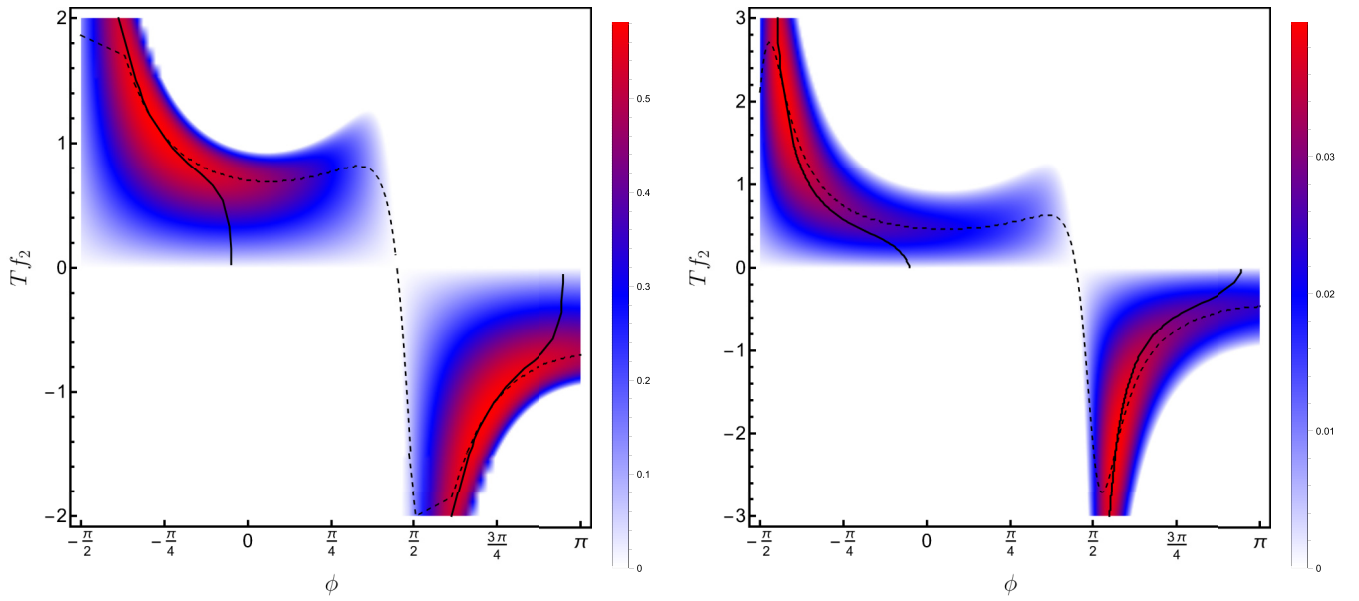

FIG. 3. For the set of drivings given by Eqs. (45) and Eq. (46) and $\tau = 2$, left and right panels depict the phase diagram of the output force $X_2 = Tf_2$ versus the phase difference ϕ for the efficiency and power output, respectively. Continuous and dashed lines denote the maximization with respect to f_2 and ϕ, respectively. Their crossings provide the simultaneous maximizations. In all cases, we set $X_1 = Tf_1 = 1$, $\gamma = k_B = m = 1$, and $T = 1/2$.

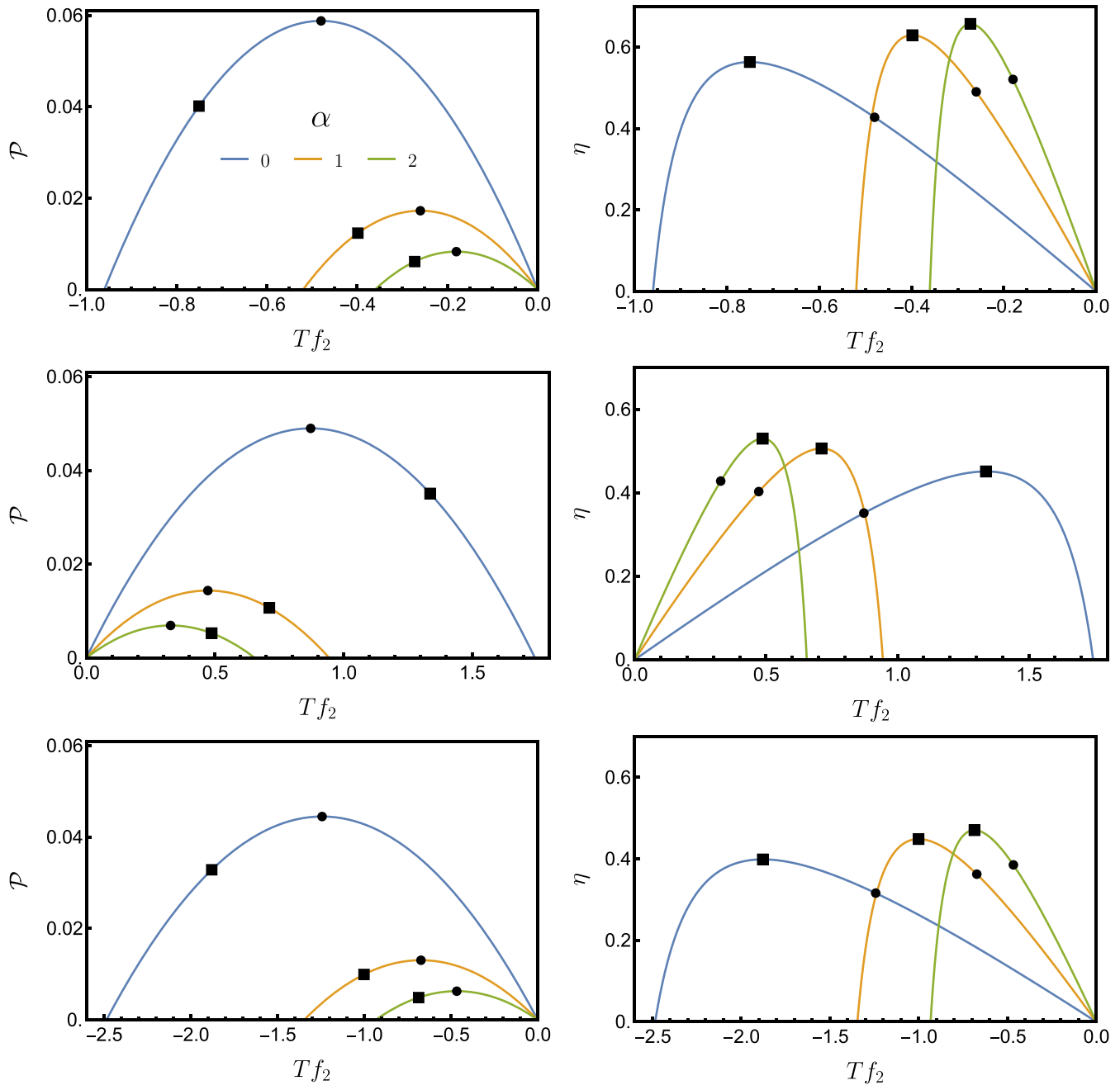

FIG. 4. For power-law drivings, the depiction of power output $\mathcal{P}$ and efficiency η versus $X_2 = Tf_2$ for representative values of α and β (from top to bottom, $\beta = 0$, 1, and 2). From the left to right curves (left side), the results for $\alpha = 0$, 1, and 2, respectively. Squares and circles denote the maximum efficiencies and powers, according to Eqs. (32) and (31). In all cases, we set $X_1 = Tf_1 = 1$, $\tau = \gamma = k_B = m = 1$, and $T = 1/2$.

1. Generic harmonic driving forces

In this section, we apply the sequential engine under a general periodical driving, having its form and strength in each half stage expressed in terms of its Fourier components:

$$g_i(t) = \sum_{n=0}^{\infty} \left[a_n^{(i)} \cos\left(\frac{4\pi n}{\tau} t\right) + b_n^{(i)} \sin\left(\frac{4\pi n}{\tau} t\right) \right], \quad (41)$$

for the ith stage ($i = 1$ or 2), where coefficients $a_0^{(i)}$, $a_n^{(i)}$, and $b_n^{(i)}$ are given by

$$a_0^{(i)} = \frac{2}{\tau} \int_{(i-1)\tau/2}^{i\tau/2} g_i(t')dt', \quad (42)$$

$$a_n^{(i)} = \frac{4}{\tau} \int_{(i-1)\tau/2}^{i\tau/2} g_i(t') \cos\left(\frac{4\pi n}{\tau} t'\right) dt', \quad (43)$$

$$b_n^{(i)} = \frac{4}{\tau} \int_{(i-1)\tau/2}^{i\tau/2} g_i(t') \sin\left(\frac{4\pi n}{\tau} t'\right) dt'. \quad (44)$$

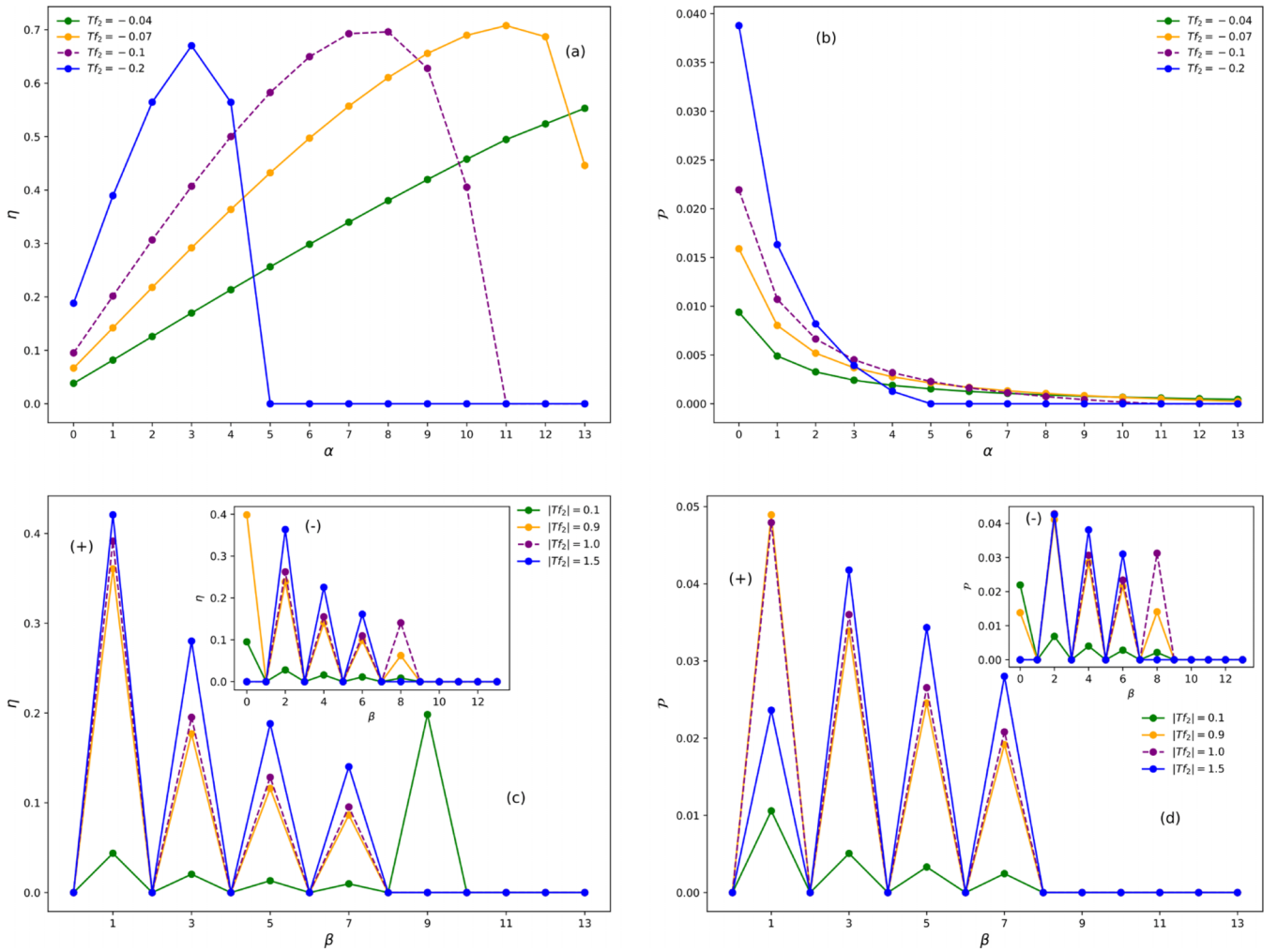

FIG. 5. For fixed forces $X_2 = Tf_2$, the depiction of efficiency (a) η and (c) $\mathcal{P}$ versus α ($\beta = 0$). Panels (b) and (d) show the same, but β is varied (for fixed $\alpha = 0$). Main panels (insets) in panels (c) and (d) show the results for odd (even) β. In all cases, we set $X_1 = Tf_1 = 1$, $\tau = \gamma = k_B = m = 1$, and $T = 1/2$.

Thermodynamic quantities and maximizations are also exactly obtained from Onsager coefficients, depending on Fourier coefficients $a_0^{(i)}$, $a_n^{(i)}$, and $b_n^{(i)}$, whose associate expressions are listed in Appendix A. To tackle the role of the driving we shall restrict ourselves to the simplest case in which drivings at each stroke have the same frequency, but different phase ϕ:

$$g_1(t) = \sin\left(\frac{4\pi}{\tau}t\right), \tag{45}$$

$$g_2(t) = \sin\left(\frac{4\pi}{\tau}t - \phi\right). \tag{46}$$

The inclusion of a lag ϕ in the second half stage has been inspired in recent works revealing that it can control of power, efficiency [7], and dissipation [60] and also by guiding the operation modes of the engine [7]. Note that ϕ corresponds to the driving parameter δ mentioned before. Figure 1 depicts some features for distinct Tf_2 and ϕ, respectively. First of all, the regime operation is delimited between zero and $|f_{2m}|$ in which maximization obeys Eqs. (31) [acquiring the simpler form given by Eq. (47), as shown below] and a similar expression (although cumbersome) is obtained for f_{2ME}/f_1. Note that, for $\gamma\tau \ll 1$ and $\gamma\tau \gg 1$, $f_{2MP}/f_1 \to 1/(2\cos\phi)$ and 0, respectively, and so the latter being independent of the lag.

$$\frac{f_{2MP}}{f_1} = \frac{4\pi(e^{\frac{\gamma\tau}{2}}+1)[2\pi\cos(\phi) - \gamma\tau\sin(\phi)]}{\gamma\tau[(e^{\frac{\gamma\tau}{2}}-1)(\gamma^2\tau^2+4\pi^2) - 4\gamma\tau(e^{\frac{\gamma\tau}{2}}+1)\sin^2(\phi)] + 16\pi^2(e^{\frac{\gamma\tau}{2}}+1)\cos^2(\phi)}, \tag{47}$$

Figure 2 reveals additional (and new) features coming from the lag in the second stage. First there is the existence of two distinct engine regimes for the some values of Tf_2, being delimited between two intervals $\phi_{1m} \leqslant \phi \leqslant \phi_{2m}$ and $\phi_{3m} \leqslant$

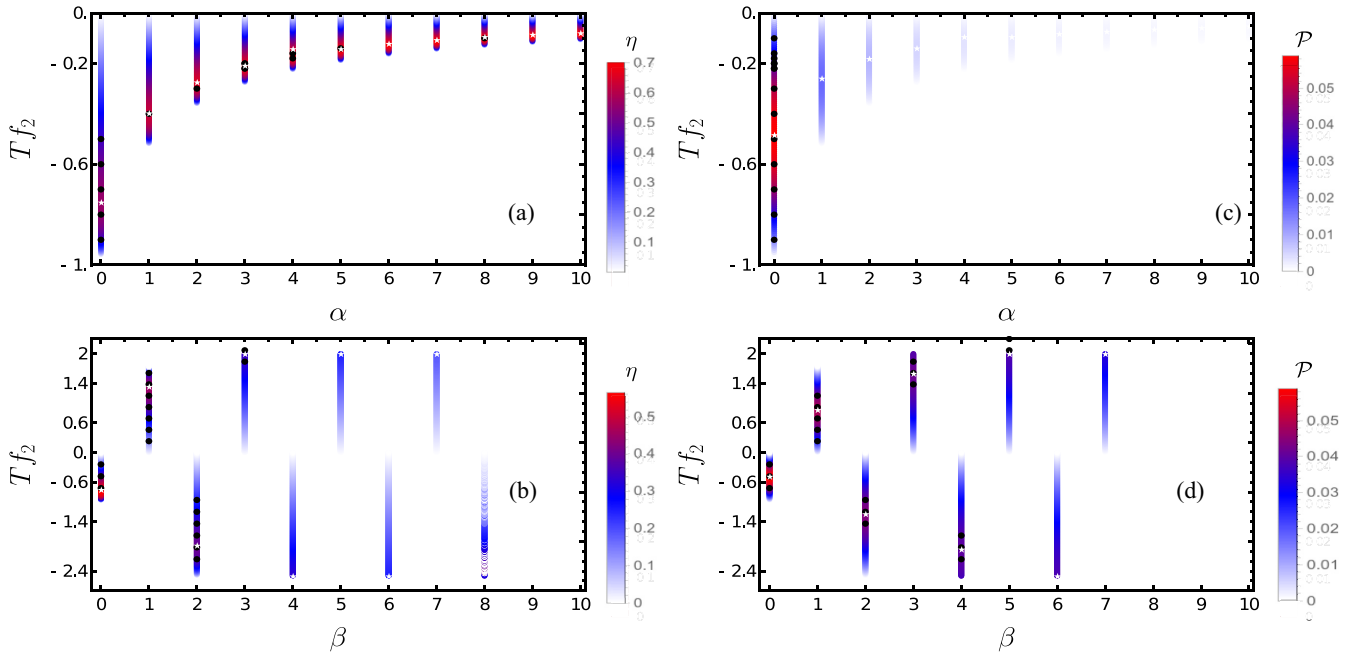

FIG. 6. Panels (a) and (c) depict, for $\beta = 0$, the phase diagram $X_2 = Tf_2$ versus α by considering the (a) efficiency and (c) power. In panels (b) and (d) is the opposite case (β is varied for fixed $\alpha = 0$). White and black symbols denote some representative maximizations with respect to the f_2 and driving (for f_2 held fixed), respectively. In all cases, we set $X_1 = Tf_1 = 1$, $\tau = \gamma = k_B = m = 1$, and $T = 1/2$.

$\phi \leqslant \phi_{4m}$ (fulfilling $\mathcal{P} = 0$ at $\phi = \phi_{im}$). Second, the change of lag moves the engine regime from positive to negative of f_2. For example, for $\tau = 2$ the engine regime yields for positive (negative) output forces for $-\pi/2 < \phi \leqslant \pi/2$ ($\pi/2 < \phi \leqslant \pi$). Finally, in similarity with coupled harmonic chains [7], the lag also controls the engine performance, having optimal ϕ_{ME} and ϕ_{MP} in which $\eta_{ME,\phi}$ and $\mathcal{P}_{MP,\phi}$, respectively. They obey Eqs. (34) and (35), the former acquiring a simpler expression

$$\frac{f_2}{f_1} = \frac{\pi[\gamma\tau \csc(\phi_{MP}) + 2\pi \sec(\phi_{MP})]}{\gamma^2\tau^2 + 4\pi^2}, \tag{48}$$

for the power and a more cumbersome (not shown) for ϕ_{ME}. In the limit of $\gamma\tau \ll 1$ and $\gamma\tau \ll 1$, Eq. (48) approaches $\phi_{MP} \to \cos^{-1}(f_1/2f_2)$ and zero, respectively. For completeness, Fig. 3 extends the aforementioned efficiency and power for other values of Tf_2 and ϕ. Note that suitable choices of ϕ and f_2 may lead to a substantial increase of engine performance. For example, for $\phi = 0$, the maximum $P_{MP,\delta=0} \approx 0.0231$ and $\eta_{ME,\delta=0} \approx 0.494$, whereas a simultaneous optimization leads to a substantial increase of power-output [given by the intersection between Eqs. (47) and (48)] $P^* \approx 0.0398$ and also of $\eta^* \approx 0.581$.

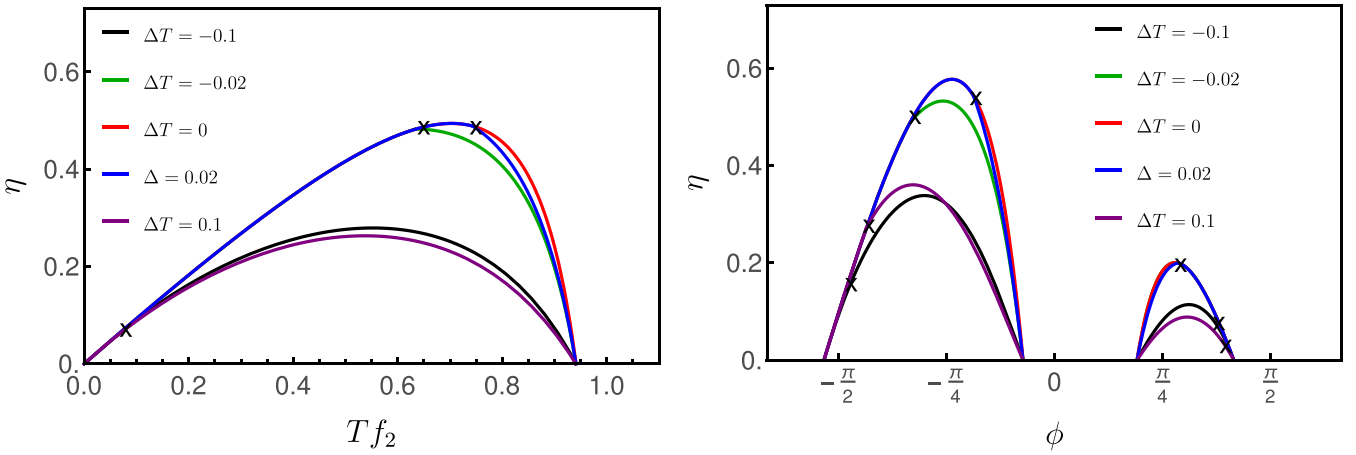

FIG. 7. For $\tau = 2$, $\phi = 0$, and $Tf_2 = 1$, the depiction of efficiency η versus Tf_2 and ϕ for distinct temperature difference ΔT between thermal baths, respectively. From top to bottom in each panel, results for distinct temperatures $\Delta T = 0, 0.02, -0.02, -0.1$, and 0.1. Symbols $\times$ attempt to the separatrix f_h/ϕ_h between the work-to-work and thermal engines, respectively. In all cases, we set $T_1 = 1/2$, $T_2 = 1/2 + \Delta T$, $X_1 = Tf_1 = 1$, and $\gamma = k_B = m = 1$.

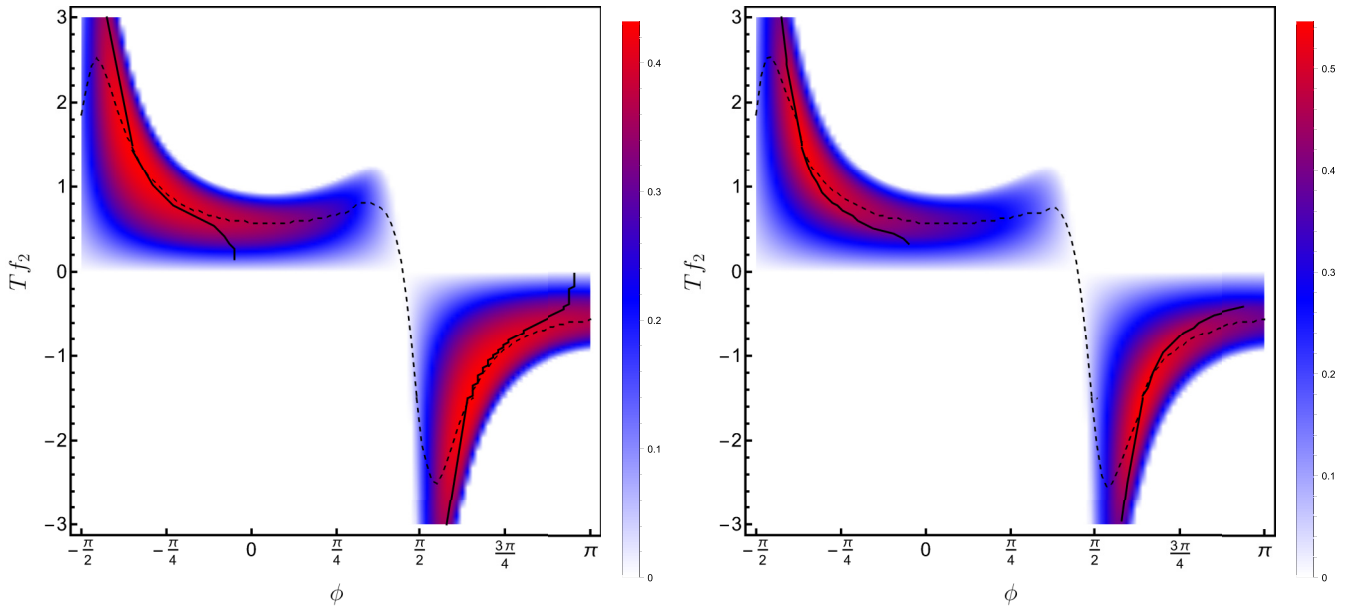

FIG. 8. For the set of drivings given by Eq. (46) and $\tau = 2$, left and right panels depict efficiency phase diagrams of the output force $X_2 = Tf_2$ versus the phase difference ϕ for $\Delta T = 0.1$ and -0.1, respectively. Continuous and dashed lines denote the maximization with respect to f_2 and ϕ, respectively. Their crossings provide the simultaneous maximizations. In all cases, we set $X_1 = Tf_1 = 1$, $\gamma = k_B = m = 1$, and $T = 1/2$.

2. *Power-law drivings*

Next we consider a general algebraic (power law) driving acting at each half stage:

$$g(t) = \begin{cases} \left(\frac{2t}{\tau}\right)^{\alpha}, & \text{for } t \in [0, \tau/2] \\ \left(1 - \frac{2t}{\tau}\right)^{\beta}, & \text{for } t \in [\tau/2, \tau], \end{cases} \tag{49}$$

where α and β assume non-negative values. This extends the analysis for Ref. [19] in which the particular cases $\alpha = \beta = 0$ and $\alpha = \beta = 1$ were considered. To exploit in more details the influence of algebraic drivings into the first (being the work source and heat source) and second (responsible for the output work $\mathcal{P}$) stages, analysis will be carried out by changing each one of them separately [i.e., keeping fixed β and α in the former and latter stages, respectively]. Although quantities can be straightforwardly obtained from Eqs. (19)–(27), expressions are very cumbersome (see, e.g., Appendix B) and for this reason analysis will be restricted to remarkable values of α and β. In principle, they can assume integer and half-integer values. Nonetheless, inspection of exact expressions reveals that Onsager coefficients assume imaginary values when β is half integer. Since half integer values α do not promote substantial changes (not shown), all analysis will be carried out for both α and β integers. Thermodynamics quantities are directly obtained from Eqs. (27), whose Onsager coefficients are listed in Appendix B.

Figure 4 depicts the main portraits of the engine performance by varying the output force for some representative values of Tf_2, α and β. First, the power output $\mathcal{P}$ (left panels) is strongly (smoothly) dependent on the shape of driving acting over the first (second) half stage. In the former case, $\mathcal{P}$ is larger for smaller α [having its maximum for time independent ones ($\alpha = \beta = 0$)] and always decreases (for all values of Tf_2) as α goes up. Unlike the substantial reduction of power output as α is raised, it is f_2 dependent as β (for fixed α) is increased, in which $\mathcal{P}_{mP,f_2}$ mildly decreases in such case. The increase of β confers some remarkable features, such as the substantial increase of range of output forces ($|f_{2m}|$ increases) in which the system operates as an engine, being restricted to positive (negative) f_2 for odd (even) values of β. Complementary findings are achieved by examining the influence of drivings for the efficiency. Unlike the $\mathcal{P}$, η is f_2 dependent but η_{mE,f_2} always increases as α is raised and mildly decreases as β goes up. Finally, we stress that η_{mE,f_2} (squares) and η_{mP,f_2} (circles) in the right panels obey Eqs. (32) and (33), respectively, having their associate $\mathcal{P}_{ME,f_2}$ and $\mathcal{P}_{MP,f_2}$ illustrated in the left panels.

Next, we tackle the opposite route, in which f_2 is kept fixed with α or β being varied in order to ensure optimal performance. Maximization of quantities follow theoretical predictions from Eqs. (34) and (35), and Fig. 5 depicts the main trends for some representative values of f_2. The dependence of driving α on the efficiency shares some similarities when compared with f_2 [Fig. 5(a)], leading to the existence of an optimal driving $\alpha > 0$ ($\alpha = 0$) for low (large) values of $|f_2|$. Hence, a driving beyond the constant case in the first stage can be important for increasing efficiency, depending on the way the machine is projected. On the other hand, for power-output purposes, $\mathcal{P}_{MP,\alpha=0}$ are always maxima and decrease for $\alpha > 0$, irrespective of the value of output force [Fig. 5(c)]. The opposite case (fixed α by varying

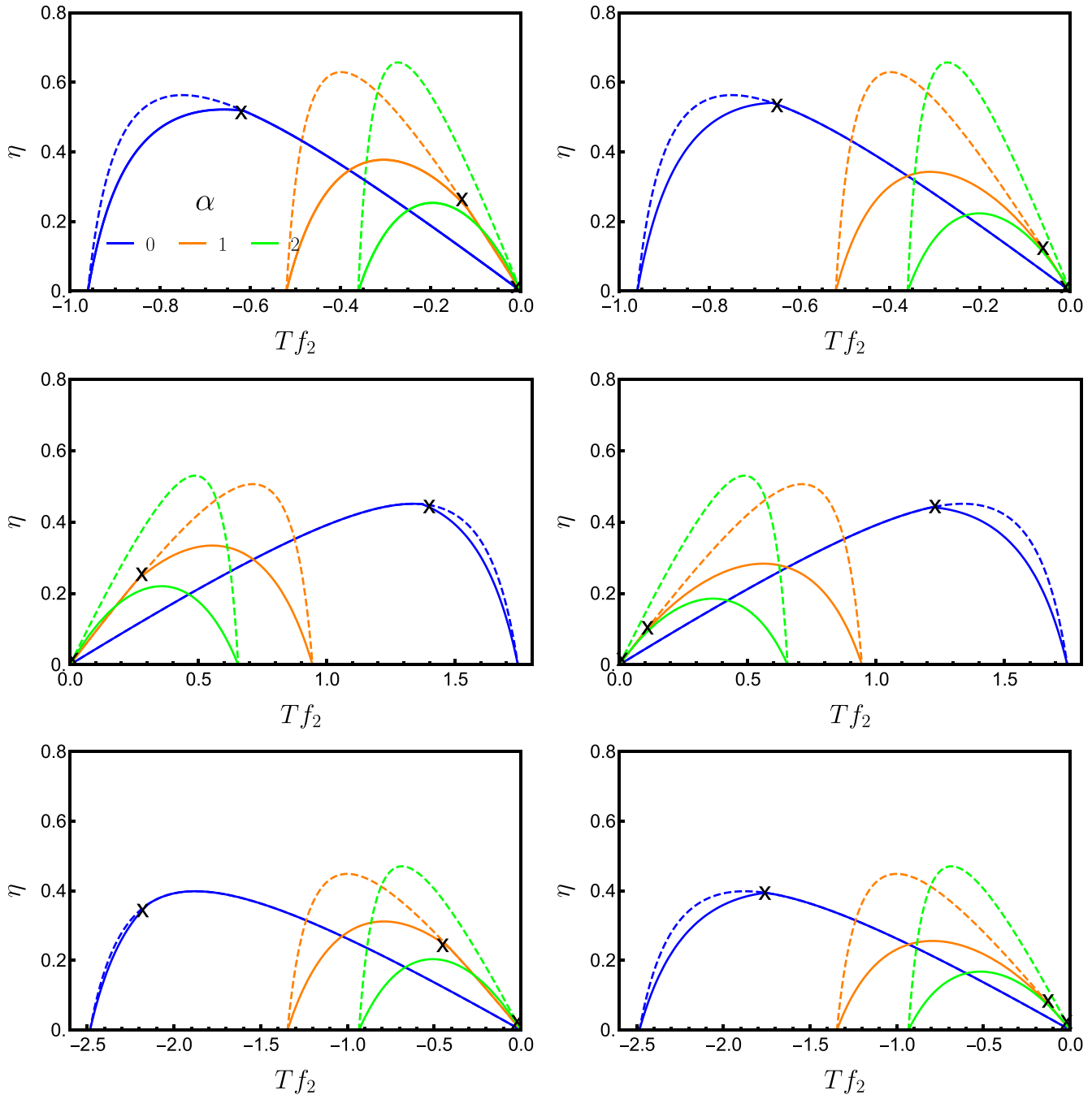

FIG. 9. Left and right panels show the efficiency η versus Tf_2 for distinct α for $\Delta T = 0.025$ and $\Delta T = -0.025$, respectively. From the left to right curves (left side), the results for $\alpha = 0$, 1, and 2, respectively. Dashed lines denote the corresponding $\Delta T = 0$ (work-to-work) engines. Symbols $\times$ denote the separatrix f_h between regimes in which the particle receive heat from the thermal bath. In such a case, efficiencies are different. From top to bottom, $\beta = 0$, 1, and 2.

β) is also more revealing and it is f_2 dependent [see, e.g., Figs. 5(c) and 5(d) and Fig. 6]. They exhibit similar behavior when β is changed. The optimal β ensuring maximum efficiencies $\eta_{mE,\beta}$ and powers $\mathcal{P}_{mP,\beta}$ also follow Eqs. (34) and (35), being f_2 dependent and even (odd) for negative (positive) f_2. They typically coincide (an exception is found for $Tf_2 = 1.5$) and occur for lower values. Figure 6 extends aforementioned findings for several values of α and β. In contrast with the harmonic drivings, a global optimization in such case has not been performed, since α and β are integers.

Summarizing the above findings: while low values for α is always more advantageous for enhancing the power output, there is a compromise between force $|f_2|$ and α and β in order to enhance the efficiency. On the other hand, although maximum efficiencies and powers smoothly decreases with β, the set of output forces $|f_2|$ in which the system operates as an engine is substantially enlarged.

C. Difference of temperatures

In this section we examine the effects of different drivings at each stroke when the temperatures are different. Although $\mathcal{P}$ does not depend on the temperature, the numerator of Eq. (29) is the same as before, now the system can receive heat from the thermal bath 1 or 2 if $T_1 > T_2$ or $T_1 < T_2$, respectively, and hence such kind of engine becomes less efficient when the difference of temperatures raises. We wish to investigate the interplay between parameters as a strategy for compensating above point. Taking into account that $\overline{\dot{Q}}_1$ (or $\overline{\dot{Q}}_2$) also depends on the f_1 and f_2, for small ΔT the system will receive heat from a thermal bath 1 (2) only if $2m\gamma \int_0^{\tau/2}\langle v_1\rangle^2 dt < \tanh(\gamma\tau/2)(T_1 - T_2)$ $[2m\gamma \int_{\tau/2}^{\tau}\langle v_2\rangle^2 dt < \tanh(\gamma\tau/2)(T_2 - T_1)]$. Hence, for a small difference in temperatures, the amount of (average) heat yields for a lower range of f_2 (or ϕ for harmonic drivings) than $|f_m|$, since $Q_i \leqslant 0$ only for some specific parameters. Let f_h (or ϕ_h) be the threshold force separating above regimes. It satisfies $\overline{\dot{Q}}_i(f_h) = 0$, implying that, for $|f_h| < |f_2| \leqslant |f_m|$ and $0 \leqslant |f_2| \leqslant |f_h|$, the system receives and does not receive heat (work-to-work converter), respectively. Hence the temperature difference is playing no role in the latter case and all previous analysis and expressions can be applied. For large ΔT (not considered here), $\overline{\dot{Q}}_i$ is always negative and the system efficiency is always lower than the work-to-work case.

Figures 7 and 8 exemplify thermal engines for harmonic drivings. As stated before, although the system operates in a similar way to the work-to-work converter for some values of Tf_2 (see, e.g., symbols $\times$ separating the thermal from work-to-work regimes), the efficiency decreases as ΔT is raised, illustrating the no conversion of heat into output work. Interestingly, the system placed in contact with the hot thermal bath in the first stage leads to somewhat higher efficiencies ($\eta^* \approx 0.547$) than in the first stage $\eta^* \approx 0.433$). This can be understood by examining the first term in the right sides of Eqs. (20) and (22). Since the contribution coming from the difference of temperatures is the same in both cases, the interplay between lag and driving forces leads $\int_0^{\tau/2}\langle v_1\rangle^2(t)dt$ to be larger than $\int_{\tau/2}^{\tau}\langle v_2\rangle^2(t)dt$ and hence conferring some advantage when $T_1 > T_2$.

Lastly, Fig. 9 extends the results for thermal engines for power-law drivings. For all values of α and β, the thermal engine is marked by a reduction of its performance as $\Delta T \neq 0$, being more substantial as α is raised and less sensitive to the increase of driving in the second state (increase of β). The engine performances also exhibit some (small) differences when the hot bath acts over the first and second strokes (see, e.g., left and right panels), being somewhat larger when $\Delta T > 0$. In such case, the interplay between driving forces leads to $\int_0^{\tau/2}\langle v_1\rangle^2(t)dt$ be lower than $\int_{\tau/2}^{\tau}\langle v_2\rangle^2(t)dt$ and hence conferring a small advantage when $T_1 < T_2$.

IV. CONCLUSIONS

The influence of the driving in a collisional approach for Brownian engine, in which the particle is subjected each half stage to a distinct force and driving, was investigated from the framework of stochastic thermodynamics. General and exact expressions for thermodynamic quantities, such as output power and efficiency were obtained, irrespective the kind of driving, period, and temperatures. Distinct routes for the maximization of power and efficiency were undertaken, whether with respect to the strength force, driving, and both of them for two kinds of drivings: generic power-law and harmonic drivings. The engine performance can be strongly affected when one considers simple (and different) power-law drivings acting over the system at each stage. While a constant driving is always more advantageous for enhancing the power output, a convenient compromise between force $|f_2|$, α, and β can be adopted for improving the efficiency. Conversely, harmonic drivings not only allows us to perform a simultaneous maximization of the engine's performance but also the change of driving (exemplified by a phase difference in the second stage) confers a second advantage, namely, a substantially enlarged engine regime. As a final comment, it is worth pointing out the decrease in engine performance as the difference of temperatures between thermal baths is increased. The inclusion of new ingredients, such as a coupling between velocity and drivings, may be a candidate in order to circumvent this fact and be responsible for a better performance of such class of collisional thermal engines. On the other hand, we highlight that the present class of engines setup suggests or can be interpreted as a new kind of work-to-work converter, operating at different temperatures.

ACKNOWLEDGMENTS

C.E.F. acknowledges financial support from São Paulo Research Foundation (FAPESP) under Grants No. 2021/05503-7 and No. 2021/03372-2. The financial support from National Council for Scientific and Technological Development (CNPq) is also acknowledged. This study was supported by the Special Research Fund (BOF) of Hasselt University under Grant No. BOF20BL17.

APPENDIX A: ONSAGER COEFFICIENTS FOR GENERIC PERIODIC DRIVING

Onsager coefficients for a generic periodic driving in each half stage are listed below:

$$L_{11} = \frac{mT}{\tau(e^{\gamma\tau}-1)}\sum_{n=0}^{\infty}\sum_{m=0}^{\infty}\left\{(e^{\gamma\tau}-1)\int_0^{\tau/2}\left[a_m^{(1)}\cos\left(\frac{4\pi m}{\tau}t\right)+b_m^{(1)}\sin\left(\frac{4\pi m}{\tau}t\right)\right]\left[a_n^{(1)}C_n^{(1)}(t)+b_n^{(1)}S_n^{(1)}(t)\right]e^{-\gamma t}dt\right.$$

$$\left.+\left[a_n^{(1)}C_n^{(1)}(\tau/2)+b_n^{(1)}S_n^{(1)}(\tau/2)\right]\left[a_m^{(1)}\overline{C}_m^{(1)}(\tau/2)+b_m^{(1)}\overline{S}_m^{(1)}(\tau/2)\right]\right\}, \tag{A1}$$

$$L_{22} = \frac{mT}{\tau(e^{\gamma\tau}-1)}\sum_{n=0}^{\infty}\sum_{m=0}^{\infty}\left\{(e^{\gamma\tau}-1)\int_{\tau/2}^{\tau}\left[a_m^{(2)}\cos\left(\frac{4\pi m}{\tau}t\right)+b_m^{(2)}\sin\left(\frac{4\pi m}{\tau}t\right)\right]\left\{a_n^{(2)}\left[C_n^{(1)}(t)-C_n^{(1)}(\tau/2)\right]\right.\right.$$
$$\left.+\, b_n^{(2)}\left[S_n^{(1)}(t)-S_n^{(1)}(\tau/2)\right]\right\}e^{-\gamma t}dt+\left\{a_n^{(2)}\left[C_n^{(1)}(\tau)-C_n^{(1)}(\tau/2)\right]+b_n^{(2)}\left[S_n^{(1)}(\tau)-S_n^{(1)}(\tau/2)\right]\right\}$$
$$\left.\times\,\left\{a_m^{(2)}\left[\overline{C}_m^{(1)}(\tau)-\overline{C}_m^{(1)}(\tau/2)\right]+b_m^{(2)}\left[\overline{S}_m^{(1)}(\tau)-\overline{S}_m^{(1)}(\tau/2)\right]\right\}\right\}, \tag{A2}$$

$$L_{12} = \frac{mT}{\tau(e^{\gamma\tau}-1)}\sum_{n=0}^{\infty}\sum_{m=0}^{\infty}\left\{a_n^{(2)}\left[C_n^{(1)}(\tau)-C_n^{(1)}(\tau/2)\right]+b_n^{(2)}\left[S_n^{(1)}(\tau)-S_n^{(1)}(\tau/2)\right]\right\}\left[a_m^{(1)}\overline{C}_m^{(1)}(\tau/2)+b_m^{(1)}\overline{S}_m^{(1)}(\tau/2)\right], \tag{A3}$$

$$L_{21} = \frac{mTe^{\gamma\tau}}{\tau(e^{\gamma\tau}-1)}\sum_{n=0}^{\infty}\sum_{m=0}^{\infty}\left[a_n^{(1)}C_n^{(1)}(\tau/2)+b_n^{(1)}S_n^{(1)}(\tau/2)\right]\left\{a_m^{(2)}\left[\overline{C}_m^{(1)}(\tau)-\overline{C}_m^{(1)}(\tau/2)\right]+b_m^{(2)}\left[\overline{S}_m^{(1)}(\tau)-\overline{S}_m^{(1)}(\tau/2)\right]\right\}, \tag{A4}$$

where we introduce the following shorthand notation involving the quantities $\overline{C}_m^{(i)}(t)$, $C_m^{(i)}(t)$, $\overline{S}_m^{(i)}(t)$, and $S_m^{(i)}(t)$:

$$C_n^{(1)}(t) = \int_0^t e^{\gamma t'}\cos\left(\frac{4\pi n}{\tau}t'\right)dt', \tag{A5}$$

$$\overline{C}_n^{(1)}(t) = \int_0^t e^{-\gamma t'}\cos\left(\frac{4\pi n}{\tau}t'\right)dt', \tag{A6}$$

$$S_n^{(1)}(t) = \int_0^t e^{\gamma t'}\sin\left(\frac{4\pi n}{\tau}t'\right)dt', \tag{A7}$$

$$\overline{S}_n^{(1)}(t) = \int_0^t e^{-\gamma t'}\sin\left(\frac{4\pi n}{\tau}t'\right)dt'. \tag{A8}$$

For the particular set of drivings from Eq. (46) and considering $\omega_j = 2\pi/\tau$, Onsager coefficients reduce to the following expressions:

$$L_{11} = \frac{mT\tau\left[\gamma^3\tau^3+4\pi^2\gamma\tau+16\pi^2\coth\left(\frac{\gamma\tau}{4}\right)\right]}{4(\gamma^2\tau^2+4\pi^2)^2}, \tag{A9}$$

$$L_{22} = \frac{mT\tau\{\gamma\tau[(e^{\frac{\gamma\tau}{2}}-1)(\gamma^2\tau^2+4\pi^2)-4\gamma\tau(e^{\frac{\gamma\tau}{2}}+1)\sin^2(\phi)]+16\pi^2(e^{\frac{\gamma\tau}{2}}+1)\cos^2(\phi)\}}{4(e^{\frac{\gamma\tau}{2}}-1)(\gamma^2\tau^2+4\pi^2)^2}, \tag{A10}$$

$$L_{12} = -\frac{2\pi mT\tau\coth\left(\frac{\gamma\tau}{4}\right)[\gamma\tau\sin(\phi)+2\pi\cos(\phi)]}{(\gamma^2\tau^2+4\pi^2)^2}, \tag{A11}$$

and

$$L_{21} = \frac{2\pi mT\tau\coth\left(\frac{\gamma\tau}{4}\right)[\gamma\tau\sin(\phi)-2\pi\cos(\phi)]}{(\gamma^2\tau^2+4\pi^2)^2}, \tag{A12}$$

respectively.

APPENDIX B: ONSAGER COEFFICIENTS FOR POWER-LAW DRIVINGS

For generic algebraic (power-law) drivings, the Onsager coefficients are listed below:

$$L_{11} = \frac{mT}{\tau}\int_0^{\tau/2}\left[4^{\alpha}e^{-t}\left(\frac{t}{\tau}\right)^{\alpha}\left(\frac{(-\tau)^{-\alpha}\left[\Gamma\left(\alpha+1,-\frac{\tau}{2}\right)-\Gamma(\alpha+1)\right]}{e^{\tau}-1}+(-t)^{-\alpha}\left(\frac{t}{\tau}\right)^{\alpha}[\Gamma(\alpha+1,-t)-\alpha\Gamma(\alpha)]\right)\right]dt, \tag{B1}$$

$$L_{12} = \frac{mT}{\tau}\int_0^{\tau/2}\left\{(-1)^{\beta}e^{-t}2^{\alpha+\beta-1}(-\tau)^{-\beta}\operatorname{csch}\left(\frac{\tau}{2}\right)\left(\frac{t}{\tau}\right)^{\alpha}\left[\Gamma\left(\beta+1,-\frac{\tau}{2}\right)-\Gamma(\beta+1)\right]\right\}dt, \tag{B2}$$

$$L_{21} = \frac{mT}{\tau}\int_{\tau/2}^{\tau}\left[\frac{2^{\alpha}(-\tau)^{-\alpha}e^{\tau-t}\left(1-\frac{2t}{\tau}\right)^{\beta}\left[\Gamma\left(\alpha+1,-\frac{\tau}{2}\right)-\Gamma(\alpha+1)\right]}{e^{\tau}-1}\right]dt, \tag{B3}$$

and

$$L_{22} = -\frac{mT}{\tau(e^{\tau}-1)}\int_{\tau/2}^{\tau}\left(e^{\frac{\tau}{2}-t}\left(1-\frac{2t}{\tau}\right)^{\beta}\left\{\left(\frac{2}{\tau}\right)^{\beta}\left[\Gamma(\beta+1)-\Gamma\left(\beta+1,-\frac{\tau}{2}\right)\right]+(e^{\tau}-1)\left(2-\frac{4t}{\tau}\right)^{\beta}(\tau-2t)^{-\beta}\right.\right.$$
$$\left.\left.\times\,\left[\Gamma(\beta+1)-\Gamma\left(\beta+1,\frac{\tau}{2}-t\right)\right]\right\}\right)dt, \tag{B4}$$

respectively, where $\Gamma(x)$ and $\Gamma(x,y)$ denote gamma and incomplete gamma functions, respectively.

[1] M. Esposito, R. Kawai, K. Lindenberg, and C. Van den Broeck, Phys. Rev. E **81**, 041106 (2010).
[2] S. Rana, P. S. Pal, A. Saha, and A. M. Jayannavar, Phys. Rev. E **90**, 042146 (2014).
[3] I. A. Martínez, É. Roldán, L. Dinis, D. Petrov, J. M. Parrondo, and R. A. Rica, Nat. Phys. **12**, 67 (2016).
[4] J. A. Albay, Z.-Y. Zhou, C.-H. Chang, and Y. Jun, Sci. Rep. **11**, 4394 (2021).
[5] A. Gomez-Marin, T. Schmiedl, and U. Seifert, J. Chem. Phys. **129**, 024114 (2008).
[6] N. Golubeva and A. Imparato, Phys. Rev. Lett. **109**, 190602 (2012).
[7] I. N. Mamede, P. E. Harunari, B. A. N. Akasaki, K. Proesmans, and C. E. Fiore, Phys. Rev. E **105**, 024106 (2022).
[8] Y. Jun, M. c. v. Gavrilov, and J. Bechhoefer, Phys. Rev. Lett. **113**, 190601 (2014).
[9] D. M. Busiello, D. Gupta, and A. Maritan, Phys. Rev. Res. **2**, 043257 (2020).
[10] M. Esposito, Phys. Rev. E **85**, 041125 (2012).
[11] V. Holubec and A. Ryabov, J. Phys. A: Math. Theor. **55**, 013001 (2022).
[12] S. De Groot and P. Mazur, *Non-Equilibrium Thermodynamics* (North-Holland Publishing Company, Amsterdam, 1962).
[13] U. Seifert, Rep. Prog. Phys. **75**, 126001 (2012).
[14] C. Van den Broeck, Phys. Rev. Lett. **95**, 190602 (2005).
[15] C. Van den Broeck and M. Esposito, Phys. Rev. E **82**, 011144 (2010).
[16] L. Peliti and S. Pigolotti, *Stochastic Thermodynamics: An Introduction* (Princeton University Press, 2021).
[17] A. Rosas, C. Van den Broeck, and K. Lindenberg, Phys. Rev. E **96**, 052135 (2017).
[18] A. Rosas, C. Van den Broeck, and K. Lindenberg, Phys. Rev. E **97**, 062103 (2018).
[19] A. L. L. Stable, C. E. F. Noa, W. G. C. Oropesa, and C. E. Fiore, Phys. Rev. Res. **2**, 043016 (2020).
[20] C. E. F. Noa, A. L. L. Stable, W. G. C. Oropesa, A. Rosas, and C. E. Fiore, Phys. Rev. Res. **3**, 043152 (2021).
[21] P. E. Harunari, F. S. Filho, C. E. Fiore, and A. Rosas, Phys. Rev. Res. **3**, 023194 (2021).
[22] C. H. Bennett, Int. J. Theor. Phys. **21**, 905 (1982).
[23] K. Maruyama, F. Nori, and V. Vedral, Rev. Mod. Phys. **81**, 1 (2009).
[24] T. Sagawa, J. Stat. Mech. (2014) P03025.
[25] J. M. Parrondo, J. M. Horowitz, and T. Sagawa, Nat. Phys. **11**, 131 (2015).
[26] G. Verley, M. Esposito, T. Willaert, and C. Van den Broeck, Nat. Commun. **5**, 4721 (2014).
[27] T. Schmiedl and U. Seifert, Europhys. Lett. **81**, 20003 (2008).
[28] M. Esposito, K. Lindenberg, and C. Van den Broeck, Phys. Rev. Lett. **102**, 130602 (2009).
[29] B. Cleuren, B. Rutten, and C. Van den Broeck, Eur. Phys. J. Spec. Top. **224**, 879 (2015).
[30] U. Seifert, Phys. Rev. Lett. **106**, 020601 (2011).
[31] Y. Izumida and K. Okuda, Europhys. Lett. **97**, 10004 (2012).
[32] V. Holubec, J. Stat. Mech. (2014) P05022.
[33] M. Bauer, K. Brandner, and U. Seifert, Phys. Rev. E **93**, 042112 (2016).
[34] K. Proesmans, C. Driesen, B. Cleuren, and C. Van den Broeck, Phys. Rev. E **92**, 032105 (2015).
[35] K. Proesmans, Y. Dreher, M. c. v. Gavrilov, J. Bechhoefer, and C. Van den Broeck, Phys. Rev. X **6**, 041010 (2016).
[36] V. Holubec and A. Ryabov, Phys. Rev. E **92**, 052125 (2015).
[37] R. S. Johal, Phys. Rev. E **100**, 052101 (2019).
[38] A. Purkayastha, G. Guarnieri, S. Campbell, J. Prior, and J. Goold, Quantum **6**, 801 (2022).
[39] P. H. Jones, O. M. Maragò, and G. Volpe, *Optical Tweezers: Principles and Applications* (Cambridge University Press, 2015).
[40] J. A. Albay, G. Paneru, H. K. Pak, and Y. Jun, Opt. Express **26**, 29906 (2018).
[41] A. Kumar and J. Bechhoefer, Appl. Phys. Lett. **113**, 183702 (2018).
[42] G. Paneru and H. Kyu Pak, Adv. Phys.: X **5**, 1823880 (2020).
[43] J. Li, J. M. Horowitz, T. R. Gingrich, and N. Fakhri, Nat. Commun. **10**, 1666 (2019).
[44] S. Krishnamurthy, S. Ghosh, D. Chatterji, R. Ganapathy, and A. Sood, Nat. Phys. **12**, 1134 (2016).
[45] V. Blickle and C. Bechinger, Nat. Phys. **8**, 143 (2012).
[46] P. A. Quinto-Su, Nat. Commun. **5**, 5889 (2014).
[47] A. C. Barato and U. Seifert, Phys. Rev. X **6**, 041053 (2016).
[48] K. Proesmans and J. M. Horowitz, J. Stat. Mech. (2019) 054005.
[49] V. Holubec and A. Ryabov, Phys. Rev. Lett. **121**, 120601 (2018).
[50] T. Tomé and M. J. De Oliveira, *Stochastic Dynamics and Irreversibility* (Springer International Publishing Switzerland, 2015).
[51] T. Tomé and M. J. de Oliveira, Phys. Rev. E **82**, 021120 (2010).
[52] D. M. Busiello, C. Jarzynski, and O. Raz, New J. Phys. **20**, 093015 (2018).
[53] S. Liepelt and R. Lipowsky, Phys. Rev. Lett. **98**, 258102 (2007).
[54] S. Liepelt and R. Lipowsky, Phys. Rev. E **79**, 011917 (2009).
[55] D. M. Busiello and C. E. Fiore, arXiv:2205.00294.
[56] H. Hooyberghs, B. Cleuren, A. Salazar, J. O. Indekeu, and C. Van den Broeck, J. Chem. Phys. **139**, 134111 (2013).
[57] K. Proesmans and C. Van den Broeck, Chaos **27**, 104601 (2017).
[58] A. Hensel and C. Schick, Thermochim. Acta **304-305**, 229 (1997).
[59] S. L. Simon and G. B. McKenna, J. Chem. Phys. **107**, 8678 (1997).
[60] B. A. N. Akasaki, M. J. de Oliveira, and C. E. Fiore, Phys. Rev. E **101**, 012132 (2020).